A Bifunctional Saddle-Shaped Small Molecule as a Dopant-Free Hole Transporting Material and Interfacial Layer for Efficient and Stable Perovskite Solar Cells

Xue Lai, Fei Meng, Qian-Qian Zhang, Kai Wang, Gongqiang Li, Yaping Wen, Haibo Ma,* Wenhui Li, Xianqiang Li, Aung Ko Ko Kyaw,* Kai Wang, Xiao Wei Sun, Mengzhen Du, Xiao Guo, Jianpu Wang, and Wei Huang*

Herein, a new bifunctional saddle-shaped organic small molecule named 2,2′,7,7′-tetrakis(N, N-di-p-methoxyphenyl-aniline)-α, β-cycloocta[1,2-b:4,3-b′:5,6-b′:8,7-b‴]tetrathiophenyl (α, β-COTh-Ph-OMeTAD) is synthesized. When compared with spiro-OMeTAD, a star hole transporting material (HTM) for highly efficient perovskite solar cells, the new material has a deeper highest occupied molecular orbital (HOMO) energy level of −5.30 eV, and a higher hole mobility of 2.88×10^{-4} $cm^2 V^{-1} s^{-1}$. With dopant-free α, β-COTh-Ph-OMeTAD as a HTM and an interfacial layer combinined with chlorobenzene (CB) as the anti-solvent, mesoporous perovskite solar cells (PSCs) are fabricated, which exhibit a power conversion efficiency (PCE) of 17.22% under AM 1.5 conditions, which is a little higher than that of devices based-on doped spiro-OMeTAD under the same conditions, which is 16.83%. Notably, the PSCs devices with dopant-free α, β-COTh-Ph-OMeTAD as both the HTM and interfacial layer show better stability, and after being stored in dark and dry air without encapsulation for nearly 800 h, the PCE can still be maintained at 86% of the maximum. This opens a new avenue for efficient and stable PSCs by exploring new dopant-free materials as alternatives to spiro-OMeTAD.

1. Introduction

Hybrid organic-inorganic halide perovskite materials have recently attracted tremendous research interests owing to their inherent photo-electrical properties, making them suitable light absorbers for photovoltaic devices. Within less than a decade, the power conversion efficiency (PCE) of 23.7% has reached for perovskite solar cells (PSCs) with n-i-p device structure,[1] which is comparative with that of silicon solar cells, since the first demonstration of the $CH_3NH_3PbI_3$-based liquid dye-sensitized solar cells with a PCE of 3.8% by Miyasaka et al. in 2009.[2] However, stability of PSCs is still one of the most challenges because of the perovskite layer's sensitivity to moisture and oxygen. To solve this problem, many strategies have been tried so far, such as: 1) Improving the crystallinity of perovskite films;[3–10] 2) Developing new 3D perovskite layers

X. Lai, F. Meng, K. Wang, Q.-Q. Zhang, M. Du, X. Guo, Prof. G. Li, Prof. J. Wang, Prof. W. Huang
Key Laboratory of Flexible Electronic (KLOFE) & Institute of Advanced Materials (IAM)
Jiangsu National Synergistic Innovation Center for Advanced Materials (SICAM)
Nanjing Tech University (NanjingTech)
30 South Puzhu Road, Nanjing 211816, P. R. China
E-mail: iamgqli@njtech.edu.cn

X. Lai, F. Meng, Dr. W. H. Li, Dr. X. Q. Li, Prof K. Wang, Prof X. W. Sun, Prof A. K. K. Kyaw
Guangdong University Key Laboratory for Advanced Quantum Dot Displays and Lighting
Shenzhen Key Laboratory for Advanced Quantum Dot Displays and Lighting
Department of Electrical & Electronic Engineering Southern University of Science and Technology
Shenzhen 518055, P. R. China
E-mail aung@sustc.edu.cn

Y. Wen, Prof. H. Ma
School of Chemistry and Chemical Engineering
Nanjing University
Nanjing 210023, P. R. China
E-mail haibo@nju.edu.cn

Prof. W. Huang
Shaanxi Institute of Flexible Electronics (SIFE)
Northwestern Polytechnical University (NPU)
127 West Youyi Road, Xi'an 710072, P. R. China

The ORCID identification number(s) for the author(s) of this article can be found under https://doi.org/10.1002/solr.201900011.

DOI: 10.1002/solr.201900011

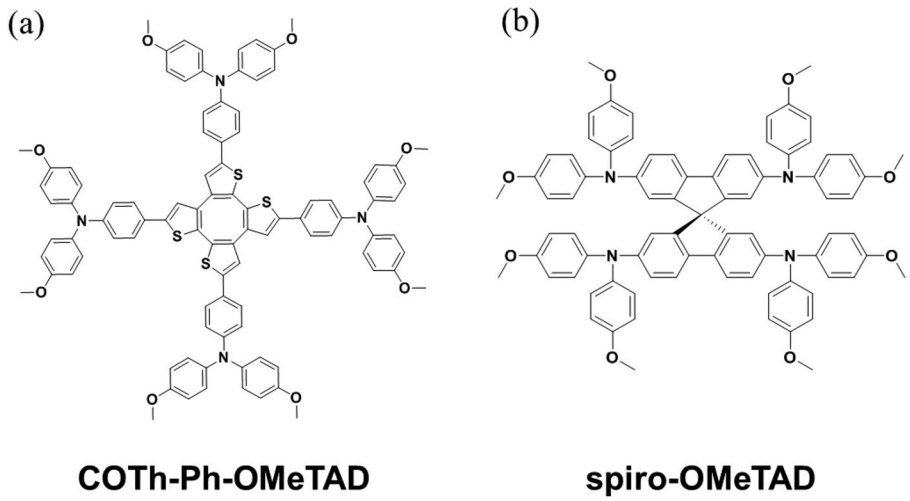

Figure 1. Structures of α, β-COTh-Ph-OMeTAD (a) and spiro-OMeTAD (b)

including all-inorganic perovskite[11–13] and quasi-2D perovskite;[14,15] 3) Developing high efficient and hydrophobicity transport materials including organic[16–20] and inorganic ones;[21] and 4) Using organic molecules doping perovskite layer on body[22–24] and surface[25,26] and so on. Among those strategies, designing new organic HTMs and doping perovskite layer with organic molecules should be efficient ways to achieve stable PSCs with high PCE, because that 1). organic molecules are more easily to be modified by tuning the HOMO/LUMO and charge mobility to fit the perovskite better, which is crucial for the effective hole transport from the perovskite absorber to the metal electrode and the resultant photovoltaic performance;[27–30] 2) organic molecules can form a hydrophobicity film, which enhance the stability of PSCs by blocking the moisture and oxygen react with perovskite layer. Thus far, 2,2′,7,7′-tetrakis(N, N-di-p-methoxyphenyl-amine)-9,9′-spirobifluorene (spiro-OMeTAD) (**Figure 1**b) is the most featured and commonly used HTM for highly efficient PSCs. It offers appropriate energy level to transfer hole and block electron from the perovskite film, while the almost 90° twisted rigid spirobifluorene can suppress aggregation, which reduce the bimolecular combination.[5,31] However, because of poor mobility of the pristine spiro-OMeTAD, lithium bis(trifluoromethylsulphonyl)imide (Li-TFSI), or tertbutylpyridine (TBP) are usually required as oxidizing dopants to improve mobility of spiro-OMeTAD. Nevertheless, these dopants are sensitive to the moisture and oxygen, resulting in the accelerated degradation of PSCs.[32,33] Additionally, the challenging synthetic route for the spirobifluorene core along with low overall yield and costly purification makes spiro-OMeTAD relatively expensive. So, developing high efficient dopant-free HTMs has become an essential to achieve stable PSCs with high PCE.

Herein, we synthesized a new HTM named 2,2′,7,7′-tetrakis(N, N-di-p-methoxyphenyl-aniline)-α, β-cycloocta[1,2-b:4,3-b′:5,6-b″8,7-b‴]tetrathiophenyl (α, β-COTh-Ph-OMeTAD) with a HOMO/LUMO energy of −5.30/−2.91 eV as shown in Figure 1a, which containing a cyclooctatetrathiophene (COTh),[34–40] a saddle-shaped motif as core, and four diphenylamine units as arms. Comparing with spiro-OMeTAD as shown in Figure 1b, the new molecule may have following advantages:

1. COTh is a more flexible saddle shaped structure than that rigid spiro one in spiro-OMeTAD, which makes the confirmation of α, β-COTh-Ph-OMeTAD to fit perovskite layer better, leading to better interaction with perovskite. Meanwhile, this non-planar structure may also play a similar role as spiro unit in spiro-OMeTAD by suppressing aggregation, enhancing the extraction of holes from perovskite layer, and reducing the charge recombination.
2. The introduction of four thiophenyl units, which are common in organic semiconductors with high mobility,[41–43] can enhance hole mobility and also improve the hydrophobicity of α, β-COTh-Ph-OMeTAD, both of those may lead to more stable and higher performance of PSCs, by blocking the moisture and oxygen from perovskite layer.
3. The "S" atoms containing in α, β-COTh-Ph-OMeTAD, as a Lewis base, may react with perovskite layer on surface by trap passivation,[25,26,44] to enhance the stability of perovskite layer;

Inspiring by those ideas, we fabricated the PSC with mixed-perovskite $(CsPbI_3)_{0.05}(FAPbI_3)_{0.79}(MAPbBr_3)_{0.16}$ as light absorber and α, β-COTh-Ph-OMeTAD as dopant-free HTM and interfacial layer (IL). After optimization of conditions, a best PCE of 17.22% under AM 1.5G illumination was achieved, which is higher than that of controlled PSC with doped spiro-OMeTAD as HTM in same condition. More interestingly, with a solution of α, β-COTh-Ph-OMeTAD in CB (1 mg mL^{-1}) as anti-solvent, the morphology of perovskite is changed with smaller domain size, less grain boundary, and better hydrophobicity of surface. As a result, the stability of devices are much enhanced, even after nearly 800 h without any encapsulation, the PCE is still maintained at 86% of the maximum efficiency.

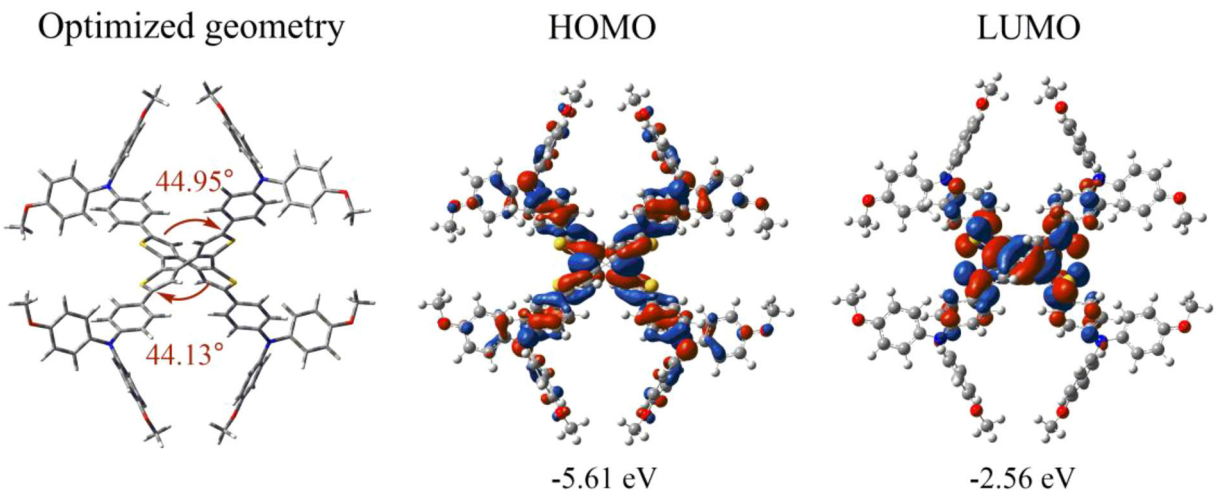

Figure 2. Optimized structure and electronic distribution in the frontier molecular orbitals of α, β-COTh-Ph-OMeTAD.

2. Results and Discussion

2.1. Synthesis and Material Properties

As shown in Scheme S1, Supporting Information, the compound α, β-COTh-Ph-OMeTAD was synthesized by Suzuki cross-coupling from (N, N-bis(4-Methoxyphenyl)-4-(4,4,5,5-tetraMethyl-1,3,2-dioxaborolan-2-yl)) and 2,5,8,11-tetrabromocyclooocta[1,2-b:4,3-b′:5,6-b″:8,7-b‴]-tetra-thiophene, which was synthesized in two steps by self-coupling of 3,3′-dibromo-2,2′-bithiophene and then bromination. The structure of α, β-COTh-Ph-OMeTAD was characterized by nuclear magnetic resonance (NMR), FTIR, HRMS (MALDI-TOF), and Elemental Analysis (EA) (Figure S3-6, Supporting Information). Thermogravimetric analysis (TGA) and differential scanning calorimetry (DSC) show that the thermal decomposition temperature of α, β-COTh-Ph-OMeTAD is 308 °C and its phase transition temperature is 121.5 °C (Figure S7, Supporting Information). To demonstrate the solubility of α, β-COTh-Ph-OMeTAD, different solvents such as dichloromethane, ethyl acetate, tetrahydrofuran, chlorobenzene, and toluene are tried and find that α, β-COTh-Ph-OMeTAD not only can be dissolved very well in these solvents, but also can form very good films for further device fabrications (Figure S8, Supporting Information). The UV-vis absorption spectra of

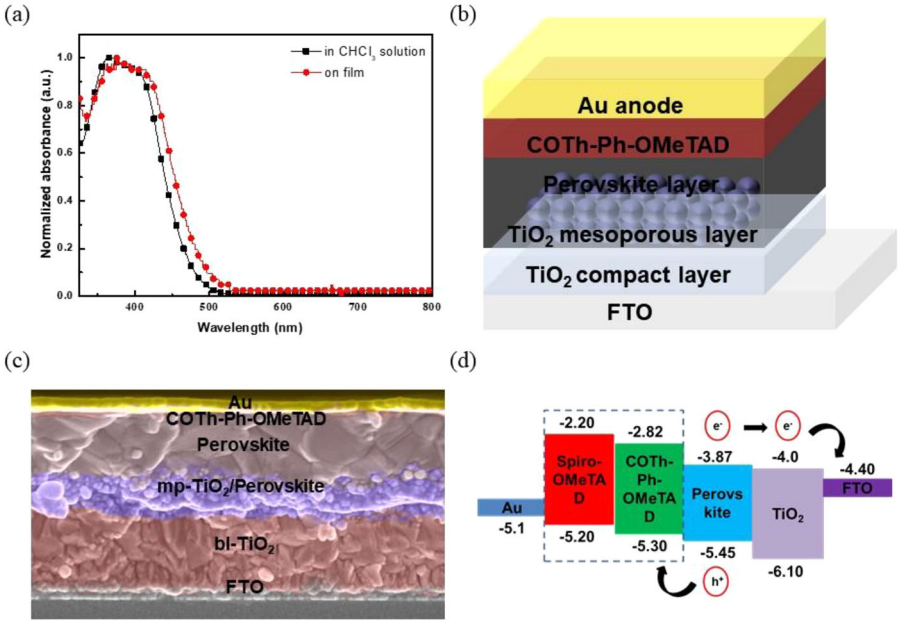

Figure 3. a) UV-vis absorption spectra of SM on glass substrate and in $CHCl_3$ solution. b) Device structure and (c) cross-sectional SEM of PSC with α, β-COTh-Ph-OMeTAD HTM. d) Energy levels of individual layers used in the device, comparing the energy levels of α, β-COTh-Ph-OMeTAD, and spiro-OMeTAD.

Table 1. Optical and electrochemical properties of SM.

	λ_{max}(sol) [nm][a)]	λ_{max}(film) [nm][b)]	$\lambda_{(UV\text{-}PL)}$(film) [nm][b)]	E_g^{opt} [eV][c)]	HOMO [eV][d)]	LUMO [eV][e)]
α, β-COTh-Ph-OMeTAD	361	375	517	2.39	−5.30	−2.91

[a)] Solution absorption spectra (1×10^{-5} M in chloroform); [b)]Absorption spectra of films on quartz glass; [c)]Optical bandgap derived from the absorption and emission intersection of small molecular films: $E_g = 1240/\lambda_{(UV\text{-}PL)}$ eV: $E_g = 1240/\lambda_{(UV\text{-}PL)}$ eV; [d)]Determined by ionization energy measurement system; [e)] $E_{LUMO} = E_{HOMO} + E_g^{opt}$.

α, β-COTh-Ph-OMeTAD in chloroform and thin film on a quartz substrate are showed in **Figure 3**a. The absorption band maximum is located at 361 nm in solution whereas at 375 nm in film, showing a slight red shift in film due to an enhanced intermolecular interaction, and an optical bandgap is estimated to be 2.39 eV based on the absorption and emission intersection of small molecular films at 517 nm (Figure S13, Supporting Information). The highest occupied molecular orbital (HOMO) energy level of α, β-COTh-Ph-OMeTAD is −5.30 eV, which is determined by the ionization energy measurement (Figure S9, Supporting Information), and the lowest unoccupied molecular orbital (LUMO) is −2.91 eV calculated from the HOMO energy and optical bandgap. All the optical and electrochemical properties are summarized in **Table 1**. Comparing with spiro-OMeTAD (Figure 3d), the HOMO energy level of SM (−5.30 eV) is deeper, and make it better to match with the valence band edge of perovskite, which is favorable for hole extraction from perovskite. Meanwhile, the LUMO level of SM (−2.91 eV) is high enough to block the electron injection from conduction band edge of perovskite (−3.87 eV) and can suppress the recombination of electron and hole on the interface between HTM layer and perovskite.

To gain insights into the molecular structure and electron distribution, density functional theory (DFT) calculations were performed at the CAM-B3LYP/6-31G(d,p)[45] level using Gaussian 09 program.[46] The optimized geometry and electron distribution in the highest occupied molecular orbital (HOMO) and the lowest unoccupied molecular orbital (LUMO) for α, β-COTh-Ph-OMeTAD are displayed in **Figure 2**. The dihedral angles between the two thiophenes in COTh unit are 44.95° and 44.13°, which can effectively suppresses the intermolecular π–π aggregation and charge recombination, thereby improving extraction of holes from perovskite layer. Moreover, both HOMO and LUMO present π features. The HOMO is almost delocalized over the whole molecular skeleton, which is favorable to enhancing holes transfer integral, while the LUMO are mainly localized on the COTh unit and the distribution over the four triphenylamine units is negligible, which implies that α, β-COTh-Ph-OMeTAD has a relatively low electron transport possibility. Besides the electron distribution, the HOMO energy level is another vital parameter to affect the hole injection ability. To ensure the efficient hole transfer, the HOMO energy level of HTM should be higher than the valence band (VB) edge of perovskite layer (−5.45 eV). Figure 2 shows the calculated HOMO level for α, β-COTh-Ph-OMeTAD is −5.61 eV, which is in close agreement with the experimentally measured value (−5.30 eV). The calculated value is slightly lower than the VB edge of perovskite, which may be caused by the functional error in our DFT calculations. While the LUMO energy level is higher than the conduction band of perovskite (−3.87 eV), which would be effectively inhibit the electron in perovskite back to metal electrodes via β-COTh-OMeTAD. All results indicate that α, β-COTh-Ph-OMeTAD to be a potential high efficient HTM.

To determine the hole mobility of α, β-COTh-Ph-OMeTAD, the current density-voltage characteristics of a hole-only device based on the structure of ITO/PEDOT:PSS/α,β-COTh-OMeTAD/Au was carried out and analyzed by space-charge-limited current (SCLC) model (Figure S11, Supporting Information). It was determined to be $2.88 \times 10^{-4}\,cm^2\,V^{-1}\,s^{-1}$, which is higher than pristine spiro-OMeTAD ($2.23 \times 10^{-4}\,cm^2\,V^{-1}\,s^{-1}$) but much lower than doped spir-OMeTAD ($6.15 \times 10^{-3}\,cm^2\,V^{-1}\,s^{-1}$).

2.2. α, β-COTh-Ph-OMeTAD as Dopant-Free Hole Transport Layer (HTL)

To investigate the performance of α, β-COTh-Ph-OMeTAD (shorten for "SM" here onwards) as dopant-free HTM in perovskite solar cell (PSC), the corresponding devices with a structure of FTO/compact-TiO_2/mersoporous-TiO_2/perovskite/HTM/Au and the comparable ones with doped spiro-OMeTAD as HTM are fabricated as shown in Figure 3b. The corresponding cross-section SEM image of device is also shown in Figure 3c. For all devices, the perovskite films were fabricated by one-step deposition method with CB as anti-solvent.[6] After optimization of the thickness of SM by varying the concentration of SM in CB solvent, the best PCE of 15.66% with $J_{SC} = 21.05\,mA\,cm^{-2}$, $V_{OC} = 1.04$ V and FF = 71.79% was achieved in a thickness of ≈60 nm of SM condition, which was fabricated by spin coating at 3000 rpm in a concentration of 10 mg mL^{-1}. It is competitive to that of device based on doped spiro-OMeTAD, whose PCE is 16.83% ($J_{SC} = 20.86\,mA\,cm^{-2}$, $V_{OC} = 1.13$ V, FF = 71.55%). The *J*–*V* characteristics of the champion devices based on SM and doped spiro-OMeTAD are shown in **Figure 4**a, and the average PCE of 20 devices based-on SM and doped spiro-OMeTAD is 15.21% and 16.15%, respectively. All those results show that the new saddle-shaped SM with much less dose and without any doped can also perform as well as notorious doped spiro-OMeTAD.

The hole extraction and transport properties are very important criterions for high efficiency of HTMs. To understand the hole extraction of SM from perovskite, the spectroscopy of steady state and transient photoluminescence (PL) are measured. Figure 4c shows the steady state PL spectra of bare perovskite and perovskite/HTL samples deposited on the glass substrates, where the HTL is SM with a thickness of ≈60 nm or doped spiro-OMeTAD with that of ≈270 nm as optimized before. All the samples give a same PL peak at 760 nm, which arises from the perovskite ($(CsPbI_3)_{0.05}(FAPbI_3)_{0.79}(MAPbBr_3)_{0.16}$). With SM or doped spiro-OMeTAD on the perovskite, the

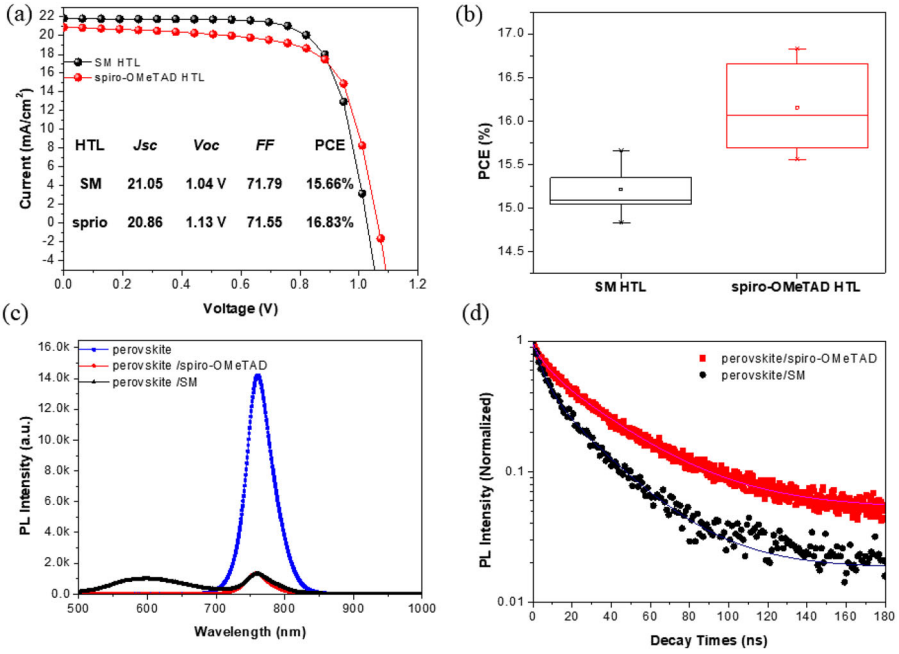

Figure 4. a) *J–V* curves measured by reverse scans of the best PSCs prepared by SM or spiro-OMeTAD as HTL with an active area of 0.11 cm^2, b) PCE statistics of PSCs prepared by SM or spiro-OMeTAD HTL, c) The steady-state PL spectra of bare perovskite film and perovskite film covered by SM or spiro-OMeTAD HTL, d) TrPL of perovskite film covered by SM or spiro-OMeTAD HTL.

intensity of the peak was significantly reduced comparing with the bare perovskite film, which is attributed to the charge extraction from perovskite to the corresponding HTM. Notably, a new peak at 597 nm in perovskite/SM film can be attributed to the PL of SM, which is confirmed by the PL of SM film (Figure S10, Supporting information). We also quantified the PL quenching efficiency (η_{quench}) due to the hole extraction of HTL from perovskite by Equation (1):[47]

$$\eta_{quench} = \frac{PL_{bare} - PL_{quench}}{PL_{bare}} \quad (1)$$

where PL_{quench} and PL_{bare} are integrated PL intensities of perovskite on glass substrate with and without HTM, respectively.We find that the PL quenching efficiency of SM (91%) is similar with doped spiro-OMeTAD (90%) (Table S1, Supporting Information), which indicates that the SM is highly efficient to extract hole from perovskite. As showed in Figure 4d, the charge dynamics of the perovskite/HTM samples (where HTL is SM or doped spiro-OMeTAD) are investigated by Time-resolved PL (TrPL) measurements with a pump laser at 450 nm, and PL signals at 760 nm standing for perovskite PL peak were collected. All the TrPL data exhibit a bi-exponential decay behavior rather than mono-exponential decay behavior and hence, all curves are fitted with bi-exponential decay as below:

$$I(t) = A_1 \exp\left(-\frac{t}{\tau_1}\right) + A_2 \exp\left(-\frac{t}{\tau_2}\right) + A_0 \quad (2)$$

where A_1 and A_2 are the relative amplitudes, τ_1 and τ_2 are the best-fit PL decay time. The faster decay time τ_1 is attributed to quenching of the photogenerated free carriers via trap states or interfacial charge transfer (between perovskite and HTM in this case), and the slower decay time τ_2 is described to the radiative recombination of free carrier which usually reflects the carrier lifetime in perovskite film.[48] In the case of the sample of perovskite/SM, it has a much shorter average lifetime of 23.48 ns with $\tau_1 = 5.05$ ns and $\tau_2 = 27.07$ ns (Table S1 Supporting Information), comparing with that of sample of perovskite/doped spiro-OMeTAD, in which the average lifetime is 40.57 ns with $\tau_1 = 11.19$ ns and $\tau_2 = 46.33$ ns. The shorter τ_1 in the perovskite/SM sample implies that the interfacial charge transfer from perovskite to SM is more efficient than that from perovskite to doped spiro-OMeTAD, and also the SM can passivate trap states better than doped spiro-OMeTAD on perovskite. Despite a more efficient charge transfer and charge extraction as discussed above, the PCE of SM-based PSC is still slightly lower than that of doped spiro-OMeTAD-based PSC, which may be attributed to the hole mobility of SM (2.88×10^{-4} $cm^2 V^{-1} s^{-1}$), which is higher than the dopant-free spiro-OMeTAD (2.23×10^{-4} $cm^2 V^{-1} s^{-1}$), but lower than doped spiro-OMeTAD (6.15×10^{-3} $cm^2 V^{-1} s^{-1}$) (Figure S11, Supporting information).

2.3. α, β-COTh-Ph-OMeTAD as Bifunctional Material of HTM and IL

As literature reported, highly hydrophobic polymers[25,42] and small molecules[46,49] containing N, O atoms as sufficiently weak Lewis bases can passivate the trap state and effectively protect perovskite film from moisture and oxygen by coordinating with lead ions on the surface of perovskite,[50] which can enhance stability of devices of PSCs in humidity environment. In 2017,

Zhan and co-workers reported the first perylene diimide polymer (PPDIDTT) passivated perovskite layer.[25] With FTIR and Raman technologies, they found that even with a very bulky substituted PDI units nearby, the S of DTT can coordinated with Pb, which passivated perovskite layer. Recently, the same group reported a small molecule INIC2 (containing DTT units with two phenyl substituents nearby) to passivate the perovskite layer.[26] Those results indicated that thiophenyl units containing in polymer or small molecules, even with bulky core and branches nearby, can work well to passivate the trap states. So as mentioned in Section 1, the "S" atoms containing in α, β-COTh-Ph-OMeTAD should be an efficient Lewis base and can play similar roles by passivating trap states and blocking moisture and oxygen on surface of perovskite as that of DTT in Zhan's report.[25,26]To investigate the interaction between SM and perovskite layer further, the devices were fabricated with different concentrations of SM in CB (arranging from 0.5 to 2.0 mg mL^{-1}) as anti-solvents to form a very thin interfacial layer (IL) on surface of perovskite, then HTM layer was spin-coated on the IL. The results are summarized **Table 2**. Notably, the PSCs fabricated from anti-solvent with 1 mg mL^{-1} of SM rendered the highest PCE of 17.22% with J_{SC} = 21.51 mA cm^{-2}, V_{OC} = 1.05 V, and FF = 76.37%, which is higher than that of device fabricated from pure CB as anti-solvent (discussed in the Section 2.2, PCE = 15.66%), and even a little higher than the controlled device with doped sprio-OMeTAD HTM (PCE = 16.83%). This demonstrates that the new SM plays some key roles as additive in anti-solvent.To understand why the SM can improve the performance, various characterizations were carried out. Firstly, scanning electron microscopy (SEM) measurement was carried out to detect the change of morphology of perovskite layer after treated with the solution of SM in CB. **Figure 5**c shows the top-view SEM images of perovskite layer fabricated with only CB as anti-solvent (let's denote as "perovskite (CB)") and that fabricated with a solution of SM (1 mg mL^{-1}) in CB as anti-solvent (let's denote as "perovskite (SM)") on the FTO/compact-TiO_2/mesoporous-TiO_2/perovskite. It is found that the big grain boundaries with average grain size of 200 nm appeared clearly on the surface of perovskite (CB), but which disappeared with the more homogeneous perovskite crystals on the surface of perovskite (SM). Secondly, X-ray diffraction (XRD) of perovskite (CB) and perovskite (SM) on glass substrates were carried out (Figure 5d). For both samples, the characteristic peaks for a trigonal perovskite phase at 14.12°, 20.00°, 24.58°, 28.44°, 31.88°, 35.00°, 40.64°, 43.20° marked with (−111), (−120), (021), (−222), (−231), (030), (−240), (−333), respectively, were observed with strong intensities, implying both perovskite films are highly crystalline. However, comparing with the intensities of peaks at 14.12°, 28.44° of two samples, the crystallinity of perovskite (SM) is much higher than that of perovskite (CB) at (−111), (−222) lattice planes. Meanwhile, the intensity of peak at 12.70° marked with (001) of PbI_2 cubic phase in perovskite (SM) is much smaller than that of perovskite (CB). It implies that much less PbI_2 containing in perovskite (SM) and the film is much more pure than that in perovskite (CB). Based on results from XRD and SEM, it is concluded that the addition of SM in CB can accelerate the growth of perovskite crystal to form less grain boundaries with smaller grain sizes but purer and more coverage of perovskite films, which lead to higher PCE than that without SM in CB.Steady state PL and TrPL spectra of the perovskite (CB), perovskite (SM), and perovskite (SM)/SM (SM HTM deposited on perovskite (SM)) were measured on glass substrate and analyzed as that described in Section 2.1. As shown in **Figure 6**a and b, the intensity of peak at ≈760 nm in perovskite (SM) is significantly weaker than that in perovskite (CB), and the peak in perovskite (SM)/SM is the weakest one in three of them. As shown in Table S1, both decay time τ_1 and decay time τ_2 become shorter and shorter in perovskite(CB) (τ_1 = 8.56 ns and τ_2 = 80.27 ns), perovskite(SM) (τ_1 = 3.91 ns and τ_2 = 25.66 ns), and perovskite(SM)/SM (τ_1 = 1.75 ns and τ_2 = 21.58 ns). The shorter τ_1 implies that less trap states and the faster hole transferred from perovskite into SM layer. Usually, the longer τ_2 means longer lifetime of carrier in perovskite, but here τ_2 in the perovskite (SM) is shorter than that in perovskite (CB), which maybe cause by two reasons: 1). the smaller grain sizes and boundaries in perovskite (SM) as shown in Figure 5c; 2). The treatment of a solution of SM in CB as anti-solvent allows SM to penetrate into the bulk of perovskite film, which creates a short but highly efficient way for hole transporting from perovskite to SM as illustrated in Figure 6c. Both of these reduced the diffusion length for carrier and shorten the decay time τ_2.

To investigate the change of efficiency of charge transfer, the hole mobilities are measured by SCLC and trap density (N_t) is evaluated based on SCLC (Figure S10, Supporting Information), the N_t values are from the relation the follow equation:[51]

$$V_{\mathrm{TFL}} = qN_tL^2/2\varepsilon_0\varepsilon_r \quad (3)$$

Table 2. Photovoltaic performances of PSCs by using SM or spiro-OMeTAD as HTL and CB or CB with SM as anti-solvent.

HTL	Concentration of SM in CB [mg mL^{-1}]	J_{sc} [mA cm^{-2}]	V_{oc} [V]	FF [%]	Best PCE [%]	Average PCE[a)] [%]
spiro-OMeTAD	0.0	20.86	1.13	71.55	16.83	16.15 ± 0.68
SM	0.0	21.05	1.04	71.79	15.66	15.21 ± 0.45
SM	0.5	21.29	1.02	70.03	15.27	15.14 ± 0.13
SM	1.0	21.51	1.05	76.37	17.22	16.31 ± 0.91
SM	1.5	19.66	1.04	73.42	14.99	14.88 ± 0.11
SM	2.0	20.74	0.96	72.57	14.45	14.31 ± 0.14

[a)] The average PCE was obtained from at least 20 cells.

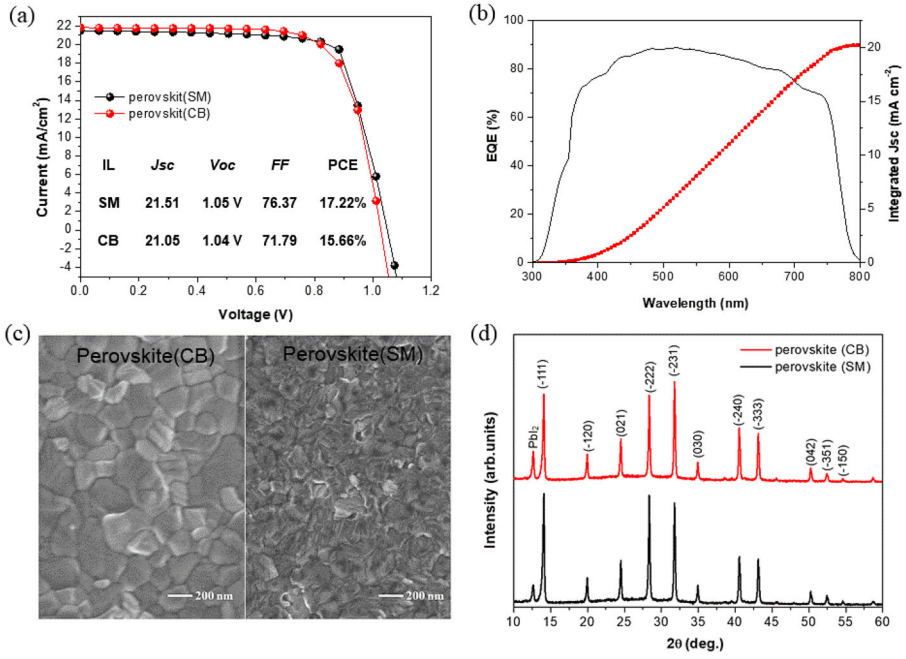

Figure 5. a) *J–V* curves measured by reverse scans of the best PSCs prepared by perovskite(CB) or perovskite(SM). SM is used as HTL and the active area of the cell is 0.11 cm^2, b) EQE spectra of the best PSC prepared by perovskite(SM) and SM HTL, c) Top surface SEM and d) X-ray diffractogram (XRD) of perovskite(CB) and perovskite (SM) film.

where represents the onset voltage of trap filled limit, q is electric charge (1.602×10^{-19} C), L is the thickness of the active layer, ε_0 is the vacuum permittivity (8.8542×10^{-14} F cm^{-1}) and ε_r is dielectric constant of perovskite (taken as the value of 32 for $MAPbI_3$ from a previous report[52]) .The trap densities of perovskite was reduced from 8.20×10^{15} cm^{-3} to 7.35×10^{15} cm^{-30}, which can be attributed to both high quality of the perovskite crystals and passivation effect from the SM. Meanwhile, the incorporation of SM in CB improved the hole mobility of perovskite (CB) from 0.162 cm^2 V^{-1} s^{-1} to 0.379 cm^2 V^{-1} s^{-1}, this can also reduce the influence about space charge, and separation of electron-hole pairs immediately after dissociating.[47]

To investigate more details about the interaction between SM and perovskite, DFT calculations are performed. As literature reported[53], the orientation of perovskite surface have a great

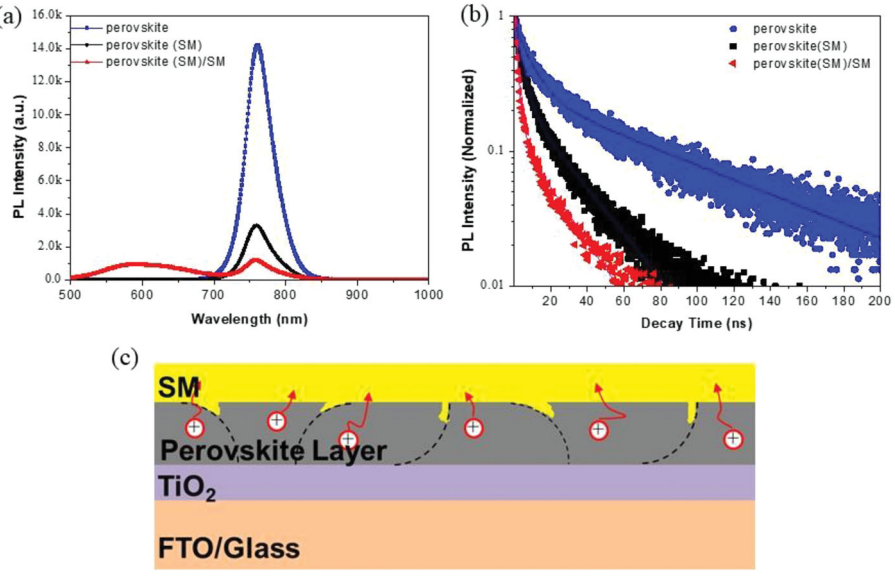

Figure 6. a) The steady-state PL spectra and (b) TrPL of perovskite(CB), perovskite(SM), and perovskite(SM)/SM, and c) the proposed hole-transport process of perovskite passivated by SM.

influence on hole/electron interfacial transfer, and the (001) and (110) surfaces tend to favor hole injection. Therefore, the perovskite (110) surface is chosen to study the interfacial properties between HTM and perovskite. To simplify the interaction model between SM and perovskite layer, the SM was instead by COTh unit and perovskite was replaced by $MAPbI_3$, and the interaction between SM and perovskite was simplified to be the core unit of α, β-COTh-Ph-OMeTAD on the defective surface of $MAPbI_3$. In order to further reduce the computational costs, the bottom two layers of the total four layers were fixed and a vacuum buffer space of 15 Å was set for slab with adsorbed atoms. Herein, a $2 \times 3 \times 4$ supercell was prepared as the adsorption surface, an I^- on its surface was removed to model a defective surface. The above configuration is geometrically optimized in VASP (Vienna ab initio simulation package[54,55] using projector-augmented wave methods with PBE[56] generalized gradient approximation (GGA)[57] exchange correlation. An energy cutoff of 500 eV was used and the force convergence criterion for geometry optimization was set to 0.02 eV $Å^{-1}$.The stable adsorption structure and the bond distance between Pb and S ($d_{Pb\text{-}S}$) as well as adsorption energy (E_{ads}) for COTh-$MAPbI_3$ complexes at the interface are plotted in **Figure 7**. The E_{ads} is defined as:

$$E_{ads} = E_{total} - E_{CH_3NH_3PbI_3} - E_{COTh} \quad (4)$$

where E_{total}, $E_{CH3NH3PbI3}$, E_{COTh} denote the energy of COTh-$MAPbI_3$ complex, clean $MAPbI_3$ and core of α, β-COTh-Ph-OMeTAD, respectively. As shown in Figure 7, the calculated *E*ads of COTh is −0.53 eV indicating the strong chemical adsorption onto the perovskite surface. In addition, the distance between S atom in the core of α, β-COTh-Ph-OMeTAD, and Pb atom on the surface is 3.09 Å, which is less than the sum of van der Waals radius of Pb and S atoms. This implies that the S atom may form a new bond with the surface Pb atom and fills the iodine vacancy of surface after adsorption to reduce trap states on perovskite surface, which benefit the transfer of hole from perovskite to HTM.

As Zhan reported, Raman tests were carried out to find the directing evidence of Pb-S, but unfortunately there was no any obvious peak in our pervoskite(SM) system because of the very low concentration of SM in anti-solvent. However, with XPS measurements as shown in Figure S14, Supporting Information, the peak of Pb shift ≈0.13 eV to right after treated with SM in CB as anti-solvent, while the peak of S at ≈164.1 eV shifted ≈0.15 eV to left, and the peak of S at ≈165.3 disappeared, those may be caused by the interaction between Pb and S.

As discussed above all, the SM in CB can not only improve crystallinity, reduce gain boundaries and sizes of perovskite, but also can form a smart interfacial layer to enhance the contact between the perovskite and HTL which help to suppress the problems associated with grain boundaries and trap states.

Beyond the enhancement of device performance, the treatment of SM in CB as anti-solvent can also improves the stability of devices. As we all know, one of the degradation mechanisms in the perovskite solar cell is the reaction between I_2 generating from the degradation of perovskite and HTM with HOMO level of around 5.0 eV, which is very close to the oxidation potential of I^-/I_3^-.[58] **Figure 8**a shows the films of SM and spiro-OMeTAD on glass substrates before and after treated (2 min) with I_2 vapor. The color of films of spiro-OMeTAD changed obviously, while that of SM films seems not change too much, exhibiting SM owning a good stability and high resistance to I_2 corrosion from the degradation of perovskite. Another degradation mechanism is related to the decomposition of the perovskite layer due to the moisture and oxygen. Figure 8c shows the contact angle measurement using deionized water droplet on

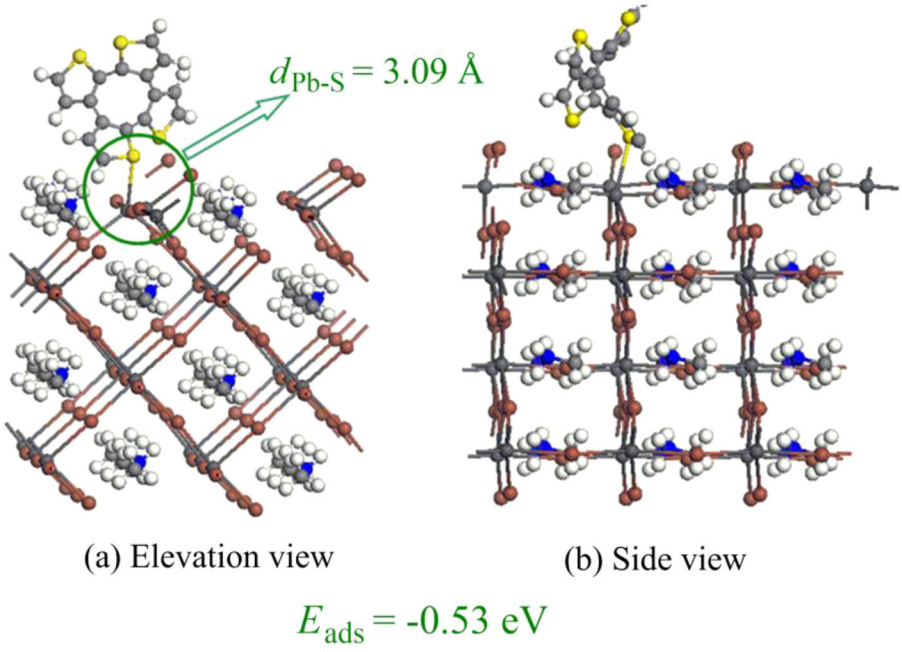

Figure 7. The optimized structure of the COTh adsorbed on the defective perovskite surface.

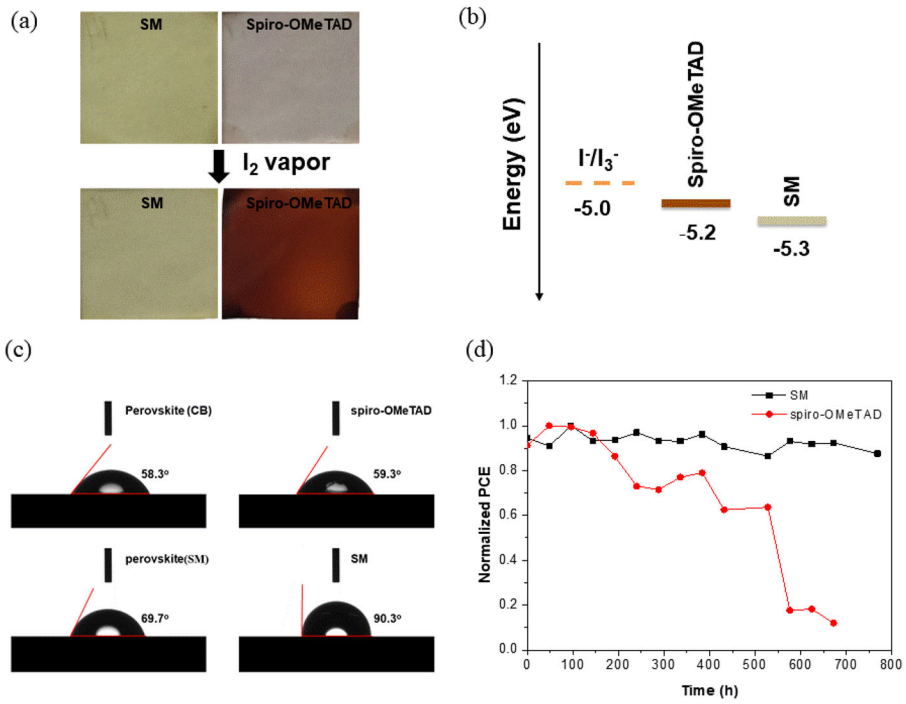

Figure 8. Color variation of SM and doped spiro-OMeTAD single films on glass before and after I_2 vapor treatment, b) Corresponding redox potential of I^-/I_3^- and the HOMO levels of spiro-OMeTAD and SM, c) the contact angles between perovskite film and water droplet on the substrate of pristine perovskite film, perovskite/spiro-OMeTAD, perovskite(SM), and perovskite(SM)/SM and d) PCE normalized to the maximum efficiencies of device with different hole transport materials stored in dark and dry air without encapsulation.

films of perovskite (CB), perovskite (SM), doped spiro-OMeTAD, and SM. The contact angle on SM film is 90.3°, which is much higher than that on spiro-OMeTAD (59.3°), exhibiting a better hydrophobic property of SM film. Moreover, the contact angle of perovskite(SM) is higher than that of perovskite (CB) (69.7° vs. 58.3°), demonstrating that the treatment of SM in CB as anti-solvent also can improve hydrophobic property of perovskite. As a result, the hydrophobic SM as interfacial layer and HTL can prevent moisture from penetrating into the perovskite and improve stability of corresponding PSCs very much. As demonstrating in Figure 8d, the PSC with SM as HTL and interfacial layer show a better stability than that with doped spiro-OMeTAD, and 86% of the maximum PCE is retained after storing for nearly 800 h in the dark and dry air, while only less than 20% of the maximum PCE is left in PSC with doped spiro-OMeTAD after storing for 600 h in same condition. More interestingly, with SM as IL and doped spiro-OMeTAD as HTL, both PCE and stability of the corresponding device are improved comparing with that of psk/Spiro-OMeTAD (Figure S15, Supporting Information), indicating that the new SM as IL is a highly efficient way to improve the stablility of PSCs.

3. Conclusion

In summary, we synthesized a new bifunctional saddle-shaped α, β-COTh-Ph-OMeTAD as both interfacial layer and dopant-free HTL for high efficient perovskite solar cells. After optimization of devices, the best PCE of 17.22% with $J_{sc} = 21.51\ mA\ cm^{-2}$, $V_{oc} = 1.05$ V, and FF = 76.37% is achieved under standard global AM 1.5 illuminations, which is very competitive to that with doped spiro-OMeTAD as HTM. More importantly, the devices with α, β-COTh-Ph-OMeTAD as interfacial layer and HTM show a much better stability, with 86% of maximum PCE retaining after storing for nearly 800 h in dark and dry air without encapsulation, than ones with doped spiro-OMeTAD as HTM (just only 20% retaining after 600 h in same condition). The mechanism of SM in devices are explored by SEM, XRD, PL, and TrPL, SCLC and theoretical calculations (DFT), all results demonstrate that the SM can enhance the crystallinity and purity of perovskite crystals, and reduce gain sizes, boundaries and trap states on surface or bulk of perovskite, which improve the charge separation and transporting and stability of PSCs. In one word, the new saddle-shaped bifunctional SM may open up a new avenue for highly efficient and stable PSCs by exploring new dopant-free materials as alternatives to spiro-OMeTAD.

4. Experimental Section

Materials: The synthetic details of the new HTMs are shown in the Supporting information.

FTO glass substrates with a sheet resistance of $15\ \Omega\ sq^{-1}$ were supplied from Advanced Election Technology Co.Ltd. MABr and FAI were purchased from Dyesol. $PbBr_2$ (99.99%), CsI (99.99%), bis (trifluoromethane) sulfonimide lithium salt (Li-TFSI, 99%), and 4-tert-butylpyridine

(tBP, 96%) were purchased from Xi'an Polymer Light Technology Corp. DMSO, DMF, acetonitrile, and CB were purchased from Sigma–Aldrich. PbI_2 (99.8%) were purchased from TCI while spiro-OMeTAD (purity. 99.5%) was purchased from Feiming Science and Technology Co., Ltd. All chemicals were used as received.

Solar Cell Fabrications: The PSCs were prepared on FTO substrates with cleaned in detergent and then successively sonicated in deionized water, acetone, and isopropyl alcohol solution, then dried in an oven at 65 °C and followed by 20 min UV-ozone treatment. The TiO_2 compact layer (bl-TiO_2) precursor solution was prepared by diluting 1 mL titanium (IV) isopropoxide in 10 mL ethanol with 12 μL HCl (12 M) and then spin coated on FTO with a rate of 6000 rpm for 30 s followed by annealing in air at 450 °C for 20 min. Subsequently, mesoporous TiO_2 (mp-TiO_2) film was spin-coated onto the FTO/bl-TiO_2 substrate using diluted commercial paste (30NR-D, Dyesol) in ethanol (150 mg mL^{-1}) at 4000 rpm and annealed at 450 °C for 20 min in air to remove the organic part.

Perovskite was deposited on FTO/bl-TiO_2/mp-TiO_2 substrate by using an anti-solvent method. To fabricate perovskite solar cells based on $(CsPbI_3)_{0.05}(FAPbI_3)_{0.79}(MAPbBr_3)_{0.16}$, the precursor solution containing FAI (1 M), PbI_2 (1.1 M), MABr (0.2 M), and $PbBr_2$ (0.2 M) in anhydrous DMF: DMSO 4:1 (v:v)[59] in glove-box. Fourty-two microliters CsI stock solution (1.5 M in DMSO) was added into the perovskite precursor solution to achieve the triple cation composition. Then, the solution was spin-coated on the FTO/bl-TiO_2/mp-TiO_2 substrates by two steps, at 1000 rpm for 10 s and 6000 rpm for 20 s, respectively, during the second step (6000 rpm), 110 μL CB or a solution of α,β-COTh-OMeTAD in CB (1 mg/mL) was pipetted onto the spinning film at 5 s before the end of this program. Then the substrates were put on a hot plate at 100 °C for 1 h. For the hole transport layer, the concentration of α, β-COTh-Ph-OMeTAD is 10 mg/ml in CB. For spiro-OMeTAD, 72 mg spiro-OMeTAD was dissolved in 1 ml CB and then added 29.2 μL of tBP, 17.6 μL of Li-TFSI (528 mg/ml in acetonitrile) and 29.2 μL tris(2-(1H-pyrazol-1-yl)-4-tert-butylpyridine) cobalt (III) tris(bis-(trifluoromethyl sulfonyl)imide) (FK209, 100 mg/ml). Both HTMs were spin coated on the perovskite layer at 3000 rpm for 30 s in glove box. Finally, 60-70 nm of gold was deposed by thermal evaporation on the top of HTL as the back electrode.

Characterization: The current density-voltage (*J–V*) of the devices were measured by a 2400 semiconductor parameter analyzer under the calibrated ABET Technologies SUN 2000 solar simulator equipped with an AM 1.5 filter at 100 mW cm^{-2}.

PL Measurements: TrPL experiments were performed using a spectrophotometer (Edinburgh Instruments FS5). For steady-state measurements, a lamp at 450 nm was used for excitation and signals were collected by a photomultiplier tube. For the dynamics, the signal was recorded at 760 nm by the time-correlated single-photon-counting detection technique. All samples were measured in air.

Supporting Information

Supporting Information is available from the Wiley Online Library or from the author.

Acknowledgements

X. L. and F. M. contributed equally to this work. Prof. G. L. thanks for the general supported by the National Key R&D Program of China (2017YFA0204704), the National Science Foundation of China (51773091, 61604069, and 61761136013), and Nature Science Foundation of Jiangsu Province (BK20171465); Prof. A. K. K. K. thanks for the general supported by Shenzhen Peacock Team Project (No. KQTD2016030111203005), Guangdong University Key Laboratory for Advanced Quantum Dot Displays and Lighting (No. 2017KSYS007) and startup fund from Thousand Young Talent Program. Prof. H. Ma thanks for the general supported by the National Science Foundation of China (21673109 and 21722302).

Conflict of Interest

The authors declare no conflict of interest.

Keywords

dopant-free, hole transporting material, interfacial layer, saddle-shaped

Received: January 9, 2019
Revised: January 31, 2019
Published online:

[1] https://www.nrel.gov/pv/assets/pdfs/pv-efficiency-chart. 2018 12171.pdf.
[2] A. Kojima, K. Teshima, Y. Shirai, T. Miyasaka, *J. Am. Chem. Soc.* **2009**, *131*, 6050.
[3] M. M. Lee, J. Teuscher, T. Miyasaka, T. N. Murakami, H. J. Snaith, *Science* **2012**, *338*, 643.
[4] M. Liu, M. B. Johnston, H. J. Snaith, *Nature* **2013**, *501*, 395.
[5] J. Burschka, N. Pellet, S. J. Moon, R. Humphry-Baker, P. Gao, M. K. Nazeeruddin, M. Gratzel, *Nature* **2013**, *499*, 316.
[6] N. J. Jeon, J. H. Noh, Y. C. Kim, W. S. Yang, S. Ryu, S. I. Seok, *Nat. Mater.* **2014**, *13*, 897.
[7] D. Shi, V. Adinolfi, R. Comin, M. Yuan, E. Alarousu, A. Buin, Y. Chen, S. Hoogland, A. Rothenberger, K. Katsiev, Y. Losovyj, X. Zhang, P. A. Dowben, O. F. Mohammed, E. H. Sargent, O. M. Bakr, *Science* **2015**, *347*, 519.
[8] Y. Liu, Z. Yang, S. Z. Liu, *Adv. Sci.* **2017**, *5*, 1700471.
[9] K. Xu, H. Ding, H. F. Lv, P. Z. Chen, X. L. Lu, H. Cheng, T. P. Zhou, S. Liu, X. J. Wu, C. Z. Wu, Y. Xie, *Adv. Mater.* **2016**, *28*, 3383.
[10] Q. F. Dong, J. F. Song, Y. J. Fang, Y. C. Shao, S. Ducharme, J. S. Huang, *Adv. Mater.* **2016**, *28*, 2816.
[11] Y. Wang, T. Zhang, M. Kan, Y. Zhao, *J. Am. Chem. Soc.* **2018**, *140*, 12345.
[12] W. Ahmad, J. Khan, G. Niu, J. Tang, *Solar RRL* **2017**, *1*, 1700048.
[13] A. Swarnkar, A. R. Marshall, E. M. Sanehira, B. D. Chernomordik, D. T. Moore, J. A. Christians, T. Chakrabarti, J. M. Luther, *Science* **2016**, *354*, 92.
[14] R. Yang, R. Z. Li, Y. Cao, Y. Q. Wei, Y. F. Miao, W. L. Tan, X. C. Jiao, H. Chen, L. D. Zhang, Q. Chen, H. T. Zhang, W. Zou, Y. M. Wang, M. Yang, C. Yi, N. N. Wang, F. Gao, C. R. McNeill, T. S. Qin, J. P. Wang, W. Huang, *Adv. Mater.* **2018**, *30*, 180477.
[15] H. Y. Zheng, G. Z. Liu, L. Z. Zhu, J. J. Ye, X. H. Zhang, A. Alsaedi, T. Hayat, X. Pan, S. Y. Dai, *Adv. Energy Mater.* **2018**, *8*, 1800051.
[16] T. Qiu, Y. Q. Hu, F. Bai, X. L. Miao, S. H. Zhang, *J. Mater. Chem. A* **2018**, *6*, 22626.
[17] J. Urieta-Mora, I. Garcia-Benito, A. Molina-Ontoria, N. Martin, *Chem. Soc. Rev.* **2018**, *47*, 8541.
[18] F. Liu, Q. Q. Li, Z. Li, *Asian J. Org. Chem.* **2018**, *7*, 2182.
[19] X.-D. Zhu, X.-J. Ma, Y.-K. Wang, Y. Li, C.-H. Gao, Z.-K. Wang,, L.-S. Liao, *Adv. Funct. Mater.* **2019**, *29*, 1807094.
[20] Y.-K. Wang, Z.-Q Jiang, L.-S. Liao, *Chin. Chem. Lett.* **2016**, *27*, 1293.
[21] Z. Yu, L. C. Sun, *Small Meth.* **2018**, *2*, 1700280.
[22] W. Q. Cai, Z. M. Chen, Z. C. Li, L. Yan, D. L. Zhang, L. L. Liu, Q-. H. Xu, Y. G. Ma, F. Huang, H-.L. Yip, Y. Cao, *ACS Appl. Mater. Interfaces* **2018**, *10*, 42564.
[23] T. Qiu, Y. Q. Hu, F. Bai, X. L. Miao, S. F. Zhang, *J. Mater. Chem. A* **2018**, *6*, 12370.
[24] H. Jiang, Z. Yan, H. Zhao, S. H. Yuan, Z. Yang, J. Li, B. Liu, T. Q. Niu, J. S. Feng, Q. Wang, D. P. Wang, H. Q. Yang, Z. K. Liu, S. Z. Frank Liu, *ACS App. Energy Mater.* **2018**, *1*, 900.

[25] F. Meng, K. Liu, S. Dai, J. Shi, H. Zhang, X. Xu, D. Li, X. Zhan, *Mater. Chem. Front.* **2017**, *1*, 1079.
[26] M. Zhang, S. Dai, S. Chandrabose, K. Chen, K. Liu, M. Qin, X. Lu, J. M. Hodgkiss, H. Zhou, X. Zhan, *J. Am. Chem. Soc.* **2018**, *140*, 14936.
[27] R. Fickler, R. Lapkiewicz, W. N. Plick, M. Krenn, C. Schaeff, S. Ramelow, A. Zeilinger, *Science* **2012**, *338*, 640.
[28] Y. J. Jeon, S. Lee, R. Kang, J. E. Kim, J. S. Yeo, S. H. Lee, S. S. Kim, J. M. Yun, D. Y. Kim, *Sci. Rep.* **2014**, *4*, 6953.
[29] K. C. Wang, J. Y. Jeng, P. S. Shen, Y. C. Chang, E. W. Diau, C. H. Tsai, T. Y. Chao, H. C. Hsu, P. Y. Lin, P. Chen, T. F. Guo, T. C. Wen, *Sci. Rep.* **2014**, *4*, 4756.
[30] N. Ahn, D. Y. Son, I. H. Jang, S. M. Kang, M. Choi, N. G. Park, *J. Am. Chem. Soc.* **2015**, *137*, 8696.
[31] Y.-K. Wang, Z.-C. Yuan, G.-Z. Shi, Y. X. Li, Q. Li, F. Hui, B. Q. Sun, Z.-Q. Jiang, L. S. Liao, *Adv. Funct. Mater.* **2016**, *26*, 1375.
[32] C. Steck, M. Franckevičius, S. M. Zakeeruddin, A. Mishra, P. Bäuerle, M. Grätzel, *J. Mater. Chem. A* **2015**, *3*, 17738.
[33] H. Chen, D. Bryant, J. Troughton, M. Kirkus, M. Neophytou, X. Miao, J. R. Durrant, I. McCulloch, *Chem. Mater* **2016**, *28*, 2515.
[34] M. J. Marsella, *Acc. Chem. Res.* **2002**, *35*, 944.
[35] Y. Wang, D. Gao, J. Shi, Y. Kan, J. Song, C. Li, H. Wang, *Tetrahedron.* **2014**, *70*, 631.
[36] C. Zhao, L. Xu, Y. Wang, C. Li, H. Wang, *Chin. J. Chem.* **2015**, *33*, 71.
[37] P. Li, Y. Lai, Y. Wang, Y. Qian, W. Duan, C. Li, Z. Wang, Q. Fang, H. Wang, B. Tu, Y. Geng, Q. Zeng, *Sci. China. Chem.* **2018**, *61*, 844.
[38] Y. Tian, G. Wang, Z. Ma, L. Xu, H. Wang, *Chem. Eur. J.* **2018**, *24*, 15993.
[39] W. Zhang, L. Xu, J. Song, Z. Ma, H. Wang, *Chin. J. Org. Chem.* **2018**, *38*, 1119.
[40] C. Zhao, X. Cai, Z. Ma, J. Shi, L. Xu, H. Wang, *J. Photochem. Photobiol., A* **2018**, *355*, 318.
[41] M. Mas-Torrent, C. Rovira, *Chem. Soc. Rev.* **2008**, *37*, 827.
[42] W. Wu, Y. Liu, D. Zhu, *Chem. Soc. Rev.* **2010**, *39*, 1489.
[43] H. Chen, W. Fu, C. Huang, Z. Zhang, S. Li, F. Ding, M. Shi, C.-Z. Li, A. K. Y. Jen, H. Chen, *Adv. Energy Mater.* **2017**, *7*, 1700012.
[44] P. L. Qin, G. Yang, Z. W. Ren, S. H. Cheung, S. K. So, L. Chen, J.-H. Hao, J. H. Hou, G. Li, *Adv. Mater.* **2018**, *30*, 1706126.
[45] T. Yanai, D. P. Tew, N. C. Handy, *Chem. Phys. Lett.* **2004**, *393*, 51.
[46] M. J. Frisch, G. W. Trucks, H. B. Schlegel, G. E. Scuseria, M. A. Robb, J. R. Cheeseman, G. Scalmani, V. Barone, B. Mennucci, G. A. Petersson, H. Nakatsuji, M. Caricato, X. Li, H. P. Hratchian, A. F. Izmaylov, J. Bloino, G. Zheng, J. L. Sonnenberg, M. Hada, M. Ehara, K. Toyota, R. Fukuda, J. Hasegawa, M. Ishida, T. Nakajima, Y. Honda, O. Kitao, H. Nakai, T. Vreven, J. A. Montgomery, J. E. Peralta Jr, F. Ogliaro, M. Bearpark, J. J. Heyd, E. Brothers, K. N. Kudin, V. N. Staroverov, R. Kobayashi, J. Normand, K. Raghavachari, A. Rendell, J. C. Burant, S. S. Iyengar, J. Tomasi, M. Cossi, N. Rega, J. M. Millam, M. Klene, J. E. Knox, J. B. Cross, V. Bakken, C. Adamo, J. Jaramillo, R. Gomperts, R. E. Stratmann, O. Yazyev, A. J. Austin, R. Cammi, C. Pomelli, J. W. Ochterski, R. L. Martin, K. Morokuma, V. G. Zakrzewski, G. A. Voth, P. Salvador, J. J. Dannenberg, S. Dapprich, A. D. Daniels, O. Farkas, J. B. Foresman, J. V. Ortiz, J. Cioslowski, D. J. Fox, *Gaussian 09, Revision D.01*. Gaussian Inc., Wallingford CT **2009**.
[47] Z. Zhu, Y. Bai, H. K. H. Lee, C. Mu, T. Zhang, L. Zhang, J. Wang, H. Yan, S. K. So, S. Yang, *Adv. Funct. Mater.* **2014**, *24*, 7357.
[48] N. De Marco, H. Zhou, Q. Chen, P. Sun, Z. Liu, L. Meng, E. P. Yao, Y. Liu, A. Schiffer, Y. Yang, *Nano Lett.* **2016**, *16*, 1009.
[49] N. K. Noel, A. Abate, S. D. Stranks, *ACS Nano* **2014**, *10*, 9815.
[50] F. Wang, S. Bai, W. Tress, A. Hagfeldt, F. Gao, *npj Flexible Electron.* **2018**, *2*, 2397.
[51] Q. Dong, Y. Fang, Y. Shao, P. Mulligan, J. Qiu, L. Cao, J. Huang, *Science* **2015**, *347*, 967.
[52] H. Tan, A. Jain, O. Voznyy, X. Z. Lan, F Pelayo Garcia de Arquer, J. A. Fan, R. Q. Bermudez, M. J. Yuan, B. Zhang, Y. C. Zhao, F. J. Fan, P. C. Li, L. N. Quan, S Hoogland, E. H. Sargent, *Science* **2017**, *355*, 722.
[53] J. Yin, D. Cortecchia, A. Krishna, S. Chen, N. Mathews, A. C. Grimsdale, C. Soci, *J. Phys. Chem. Lett.* **2015**, *6*, 1396.
[54] G. Kresse, J. Furthmüller, *Comp. Mater. Sci.* **1996**, *6*, 15.
[55] G. Kresse, J. Furthmüller, *Phys. Rev. B* **1996**, *54*, 11169.
[56] J. P. Perdew, K. Burke, M. Ernzerhof, *Phys. Rev. Lett.* **1996**, *77*, 3865.
[57] J. P. Perdew, J. A. Chevary, S. H. Vosko, K. A. Jackson, M. R. Pederson, D. J. Singh, C. Fiolhais, *Phys Rev B* **1992**, *46*, 6671.
[58] Y. Hou, X. Y. Du, S. Scheiner, D. P. McMeekin, Z. P. Wang, N. Li, M. S. Killian, H. Chen, M. Richter, I. Levchuk, N. Schrenker, E. Spiecker, T. Stubhan, N. A. Luechinger, A. Hirsch, P. Schmuki, H. P. Steinrück, R. H. Fink, M. Halik, H. J. Snaith, C. J. Brabec, *Science* **2017**, *358*, 1192.
[59] J. Jiang, Q. Wang, Z. Jin, X. Zhang, J. Lei, H. Bin, Z. G. Zhang, Y. Li, S. F. Liu, *Adv. Energy Mater.* **2018**, *8*, 1701757.